Theory of electronic properties and quantum spin blockade in a gated linear triple quantum dot with one electron spin each

Chang-Yu Hsieh,[1,2] Yun-Pil Shim,[1,3] and Pawel Hawrylak[1,2]

[1]*Quantum Theory Group, Institute for Microstructural Sciences, National Research Council, Ottawa, Canada K1A 0R6*

[2]*Department of Physics, University of Ottawa, Ottawa, Ontario, Canada, K1N 6N5*

[3]*Department of Physics, University of Wisconsin-Madison, Madison, Wisconsin 53706, USA*

(Received 17 October 2011; published 21 February 2012)

We present a theory of electronic properties and the spin-blockade phenomena in a gated linear triple quantum dot. Quadruple points where four different charge configurations are on resonance, particularly involving (1,1,1) configuration, are considered. In the symmetric case, the central dot is biased to higher energy and a single electron tunnels through the device when the (1,1,1) configuration is resonant with (1,0,1), (2,0,1), (1,0,2) configurations. The electronic properties of a triple quantum dot are described by a Hubbard model containing two orbitals in the two unbiased dots and a single orbital in the biased dot. The transport through the triple-quantum-dot molecule involves both singly and doubly occupied configurations and necessitates the description of the (1,1,1) configuration beyond the Heisenberg model. Exact eigenstates of the triple-quantum-dot molecule with up to three electrons are used to compute current assuming weak coupling to the leads and nonequilibrium occupation of quantum molecule states obtained from the rate equation. The intramolecular relaxation processes due to acoustic phonons and cotunneling with the leads are included, and are shown to play a crucial role in the spin-blockade effect. We find a quantum-interference-based spin-blockade phenomenon at low source-drain bias and a distinct spin blockade due to a trap state at higher bias. We also show that, for an asymmetric quadruple point with (0,1,1), (1,1,1,), (0,2,1), (0,1,2) configurations on resonance, the spin blockade is analogous to the spin blockade in a double quantum dot.

DOI: 10.1103/PhysRevB.85.085309 PACS number(s): 73.21.La, 73.23.Hk, 73.63.Kv

I. INTRODUCTION

Gated quantum dots[1–9] (QDs) with controlled electron numbers are a testbed for probing fundamental many-body physics as well as a promising platform for building spintronics and quantum information processing (QIP) devices.[10] Until recently, most experimental and theoretical investigations of quantum circuits based on electron spin focused on the single- and double-quantum-dot (DQD) devices.[3,10] Many essential tasks for operating a qubit have been demonstrated in DQDs. For instance, coherent manipulation and readout of one[4] and two[11] spin states have already been experimentally achieved using spin blockade.[1,12–15] In DQDs, spin blockade is used to detect spin using spin-to-charge conversion. For instance, the (0,2) charge configuration can not be obtained from the (1,1) configuration if the electron spin in the left dot is parallel to the electron spin in the right dot. Detected charge on the right dot depends on the relative spin orientations of the two electrons. Thus, spin blockade detects spin states (triplet or singlet) of the two electrons in transport spectroscopy or charge sensing measurement.[1,12,13] A physical signature of spin blockade at the triple point, $(0,1) \rightarrow (1,1) \rightarrow (0,2)$, is the current rectification under different bias directions. In positive (forward) bias direction, triplet states will not be populated, and the system does not manifest negative differential conductance (NDC). In negative (reverse) bias direction, current suppression is pronounced once the transitions to the (1,1) triplet states become accessible in the transport window.

A nontrivial extension of the quantum circuit based on electron spin is the triple quantum dot (TQD) with one electron each. This can be appreciated by the comparison of the quantum optical properties of two-level versus three-level systems. Charging and transport spectroscopy experiments[7,9,16–18] on the TQDs have already mapped out the stability diagram of the devices down to a few electrons. Recent experiments[8,19] have also demonstrated coherent manipulations of electron spins in TQDs. The electronic and transport properties of TQDs have been investigated theoretically, including topological Hunds rules,[17] spin-selective Aharonov-Bohm oscillations,[20,21] the implementation of a coded qubit,[22–24] voltage-controlled spin manipulation,[25,26] entangled GHZ state generation,[27,28] ac field control of spin blockade,[29] cotunneling-induced leakage current in blocking states,[30] non-Fermi-liquid behavior[31–33] in triangular TQDs, as well as coherent tunneling adiabatic passage[34,35] (CTAP) processes for a single electron in a linear triple quantum dot (LTQD). Many of these theoretical predictions as well as quantum information processing in a TQD require an ability to spectroscopically detect spin by, e.g., spin blockade.

In recent experiments, Granger *et al.*[16,19] and Laird *et al.*[8] carried out transport spectroscopy and charge sensing measurement on a LTQD molecule with one electron in each dot. This configuration, denoted by (1,1,1), was tuned to be resonant with the two-electron configuration (1,0,1). It was assumed that transport proceeded through {(2,0,1),(1,1,1),(1,0,2)} resonant configurations, which implied that the central dot was biased to higher energy. The presence of doubly occupied dots in the configurations makes the Heisenberg model of localized spin configurations inapplicable, and a microscopic model is required to study the electronic and transport properties of this TQD system.

Here, we extend our earlier theory of a TQD (Refs. 17, 23, 36, and 37) to biased linear molecule at quadruple

points (QPs) and describe spin blockade as a spectroscopic tool allowing the readout of electron spin. We analyze the electronic and spin properties of a LTQD as a function of energies of each dot within a single-band or multiband Hubbard model. The knowledge of the wave functions of a single-band Hubbard model allows for the qualitative understanding of the low-bias transport through the device, but including more than one orbital in the dot will be shown to be crucial for spin blockade. Two different QPs involving the (1,1,1) configuration are considered: (a) symmetrical QP (SQP) with (1,0,1),(2,0,1),(1,1,1),(1,0,2) configurations on resonance, and (b) asymmetrical QP (AQP) with (0,1,1),(1,1,1),(0,2,1),(0,1,2) configurations on resonance. For SQP, the transport goes through $(1,0,1) \rightarrow (2,0,1) \rightarrow (1,1,1) \rightarrow (1,0,2)$ channels, while $(0,1,1) \rightarrow (1,1,1) \rightarrow (0,2,1) \rightarrow (0,1,2)$ is the transport channel for the AQP. Current is calculated in sequential tunneling approximation between the TQD and the leads, using rate equations[20,38] to calculate the nonequilibrium steady-state occupation of TQD states with a source-drain bias. We use Fermi's golden rule to calculate the transition rates between TQD states by adding or removing an electron due to the coupling between the TQD molecule and the leads, and also the transition rate between TQD states with the same number of electrons due to the interaction with acoustic phonons.[39,40]

The plan of the paper is as follows. In Secs. II and II A, we describe the system, the Hamiltonian, and the electronic properties of a TQD as a function of detuning Δ of the central dot. In Sec. II B, our approach to the transport based on the sequential tunneling between the leads and the TQD molecule and rate equations are explained in detail. The transition rates due to different mechanisms are also discussed. In Sec. III A, we present results of current calculations for the SQP, and discuss the mechanism of quantum spin blockade at low bias. In Sec. III B, we present results of transport calculations for conventional spin blockade at the SQP under high source-drain bias and at the AQP, and discuss how the system at the AQP can behave qualitatively as a double dot around a similar triple point with (0,1),(1,1),(0,2) configurations. A brief conclusion is given in Sec. IV.

II. MODEL

Figure 1 presents a schematic diagram of a LTQD in contact with the two semi-infinite leads and the energy levels of the single QD orbitals. The metallic leads are modeled by one-dimensional tight-binding chains. Each quantum dot, defined by metallic gates on top of GaAlAs/GaAs heterojunction and represented here by a circle contains a controlled number of electrons, e.g., one electron each [(1,1,1) configuration] in Fig. 1(a) and (1,0,1) configuration in Fig. 1(b). Electrons can tunnel between dots 1 and 2, and between dots 2 and 3, but there is no direct tunnel coupling between the two edge dots. Figure 1(c) shows the single-particle levels of the individual dots in the LTQD without interdot tunneling. The lowest-energy bars denote S orbitals (the ground orbitals) in each dot. The energy of the central dot is raised by an applied voltage Δ. This bias can be used, for example, in order to localize the two electrons in dots 1 and 3 as shown in Fig. 1(b).

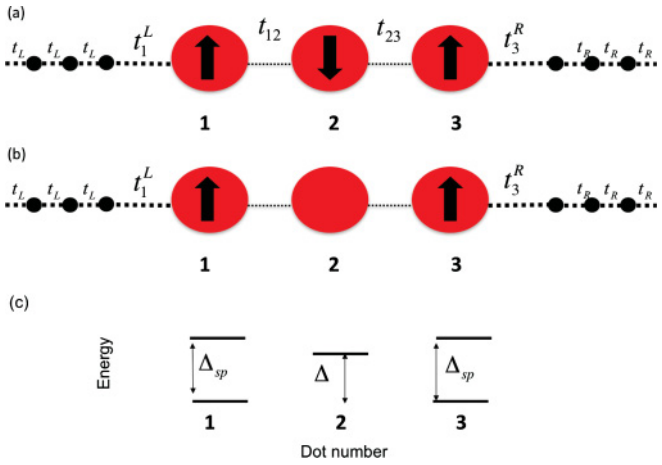

FIG. 1. (Color online) (a) Schematic picture of a LTQD with one electron spin each connected to leads. The leads are modeled with one-dimensional tight-binding chains. (b) The TQD in (1,0,1), two-electron configuration. (c) Schematic picture of single-particle energy spectrum of a TQD when the central dot is biased with Δ. The gap Δ_{sp} denotes the energy difference between the S and P orbitals on a dot.

In this study, Δ, comparable to Coulomb repulsion U, is used to bring the configurations such as (1,1,1) and (1,0,2) on resonance as shown in Fig. 2. We find it is essential to include the excited states, P orbitals, in dots 1 and 3 in order to properly account for the transport properties at the SQP. The energy separation Δ_{sp} between S and P orbitals may also be comparable to Δ. Thus, the electronic properties of a LTQD are described by a multiband Hubbard model with parameters derived from a microscopic linear combination of harmonic orbitals-configuration interaction (LCHO-CI) approach for given voltages on the gates.[36] With $\hat{c}_{i\sigma}$ ($\hat{c}_{i\sigma}^{\dagger}$) denoting annihilation (creation) operators for an electron with

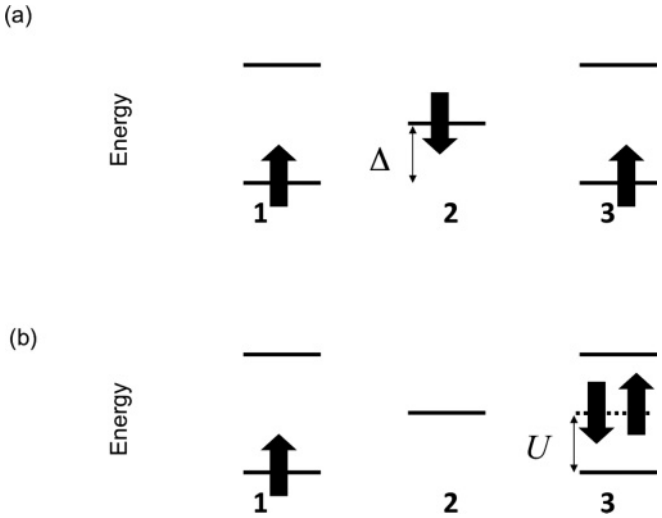

FIG. 2. Two resonant three-electron configurations in a centrally biased TQD: (a) one of the (1,1,1) singly occupied configurations and (b) one of the (1,0,2) doubly occupied configurations.

spin σ on orbital i, the five-level Hubbard Hamiltonian reads as

$$\hat{H}_D = \sum_{i=1,\sigma}^{5} E_i(V_{sd})\hat{n}_{i\sigma} + \sum_{i,j\neq i=1,\sigma}^{5} t_{ij}\hat{c}^{\dagger}_{i\sigma}\hat{c}_{j\sigma} + \sum_{i=1}^{5} U_i\hat{n}_{i\uparrow}\hat{n}_{i\downarrow} + \frac{1}{2}\sum_{i,j=1}^{5} V_{ij}\hat{\rho}_i\hat{\rho}_j, \quad (1)$$

where $E_i(V_{sd})$ is the source-drain bias dependent energy of orbital i, and t_{ij}, U_i, and V_{ij} are tunnel coupling, onsite and off-site Coulomb repulsion between orbitals i and j respectively, $\hat{n}_{i\sigma} = \hat{c}^{\dagger}_{i\sigma}\hat{c}_{i\sigma}$, and $\hat{\rho}_i = \sum_{\sigma}\hat{n}_{i\sigma}$. We assign indices $i = 1,2,3$ to S orbitals of dots 1 (left), 2 (central), and 3 (right), respectively. The indices $i = 4,5$ denote excited P orbitals. We will consider only single excited orbitals in both dot 1 ($i = 4$) and dot 3 ($i = 5$) for the TQD molecule at SQP. For the AQP case with (0,1,1) base configuration, the excited orbitals are in dot 2 ($i = 4$) and dot 3 ($i = 5$). The excited orbital in the biased dot does not play any significant role.

The TQD device is connected to left and right leads ($r = L,R$) as shown in Fig. 1(a). Electrons in the leads fill up the noninteracting states of semi-infinite tight-binding chains with a bulk dispersion relation $\epsilon_r(k) = 2t_r\cos(ka)$ up to a Fermi level $\mu_{L(R)}$, where t_r is the tunnel coupling between the sites on lead r, a is the distance between sites of tight-binding chain, and k denotes the mode of the plane wave for single-particle states in the chain. The interaction between the leads and the device is modeled as

$$\hat{H}_{rD} = \sum_{i_r,\sigma}\sum_{k}\left(\tilde{t}^{r}_{i}(k)\hat{d}^{\dagger}_{k\sigma}\hat{c}_{i_r\sigma} + \text{H.c.}\right), \quad (2)$$

where $\tilde{t}^{r}_{i}(k) = t^{r}_{i}e^{i2\pi k a m_r}/\sqrt{2\pi}$ is the tunnel coupling between the mode k of the $r = L(R)$ lead and orbital i_r localized in the left dot ($r = L$) or the right dot ($r = R$) and m_r in the exponent of $\tilde{t}^{r}_{i}(k)$ is 1 for $r = L$ and -1 for $r = R$. $\hat{d}^{\dagger}_{k\sigma}$ creates an electron with momentum k and spin σ in the lead r. In this study, $t^{R}_{i} = 0$ for orbitals not in the right edge dot and $t^{L}_{i} = 0$ for orbitals not in the left edge dot.

Interactions with phonons have already been shown to be important to understand the incoherent transport properties of double quantum dots at high bias in Ref. 40, for instance. We include interaction of electrons in the LTQD with bulk longitudinal acoustic (LA) phonons via deformation potential as the mechanism of phonon-induced relaxation at low temperature. The electron-phonon interaction Hamiltonian reads as

$$\hat{H}_{e\text{-}ph} = \sum_{i,j=1,\sigma}^{5}\sum_{q} M_{ij}(\mathbf{q})\left(\hat{b}_{\mathbf{q}} + \hat{b}^{\dagger}_{-\mathbf{q}}\right)\hat{c}^{\dagger}_{i\sigma}\hat{c}_{j\sigma}, \quad (3)$$

where $\mathbf{q}$ is the phonon momentum, i and j are TQD orbitals, and $\hat{b}_{\mathbf{q}}$ ($\hat{b}^{\dagger}_{\mathbf{q}}$) operator annihilates (creates) a phonon with momentum $\mathbf{q}$. $M_{ij}(\mathbf{q}) = \Lambda(q)\int\psi_i(r)^*\exp(-i\mathbf{q}\cdot\mathbf{r})\psi_j(r)$ is the electron-phonon scattering matrix element, $\psi_i(r)$ is a single-particle wave function, and $\Lambda(q) = \sqrt{\frac{D^2\hbar q}{2\rho c_s}}$ for deformation potential D, GaAs mass density ρ, and speed of sound c_s in GaAs. The phonon scattering matrix element $M_{ij}(\mathbf{q})$ depends on the single-particle wave function $\psi_i(r)$, which is obtained from the LCHO (Ref. 36) formalism.

A. Electronic properties of a LTQD

The electronic properties of a triangular TQD molecule with all three dots on resonance for $N = 1$–6 electrons have been described in detail in Ref. 17. We focus here on the linear molecule where there is no tunneling between the end quantum dots and on the effect of detuning Δ of the energy of the central dot. While in numerical calculations we retain all five levels, we retain only the three lowest-energy states in this semianalytical discussion of the low-energy spectra. For the Hubbard parameters, we set $U_i = U$, $t_{12} = t_{23} = t$, $t_{13} = 0$, $V_{13} = V$, and $V_{12} = V_{23} = V'$. For the onsite energies, we restrict our attention to $E_1 = E_3 = E$ and $E_2 = E + \Delta$. Since E is just an overall shift in energy, we simply set $E = 0$ until we explicitly state otherwise. The Hubbard Hamiltonian commutes with total $\hat{S}^2$ and $\hat{S}_y$, so we consider spin-resolved subspaces in the Hilbert space.

First, we focus on the single-particle molecular states of the TQD. We consider the $S_y = 1/2$ subspace and use a localized basis $\{|1\rangle,|2\rangle,|3\rangle\}$, where $|i\rangle = c^{\dagger}_{i\uparrow}|0\rangle$. In this basis, the Hubbard Hamiltonian [Eq. (1)] reads as

$$H_{1e} = \begin{bmatrix} 0 & t & 0 \\ t & \Delta & t \\ 0 & t & 0 \end{bmatrix}. \quad (4)$$

By inspection, we see that a state $|D\rangle = (|1\rangle - |3\rangle)/\sqrt{2}$, with an energy $E_D = 0$, is an eigenstate. In this state, an electron does not occupy the central dot. This state can block the transport in a setting where dots 1 and 3 are connected to the source and dot 2 is connected to the drain, and hence is called a dark state,[35,41] in analogy to the coherent population trapping in quantum optics. The existence of such a dark state can be detected by transport spectroscopy.[41] As the transport window determined by the applied source-drain voltage V_{sd} is large enough to allow the added electron to enter a dark state, a negative differential conductance should be observed in the experiment. Furthermore, Greentree *et al.*[34,42] proposed to implement CTAP to move an electron from dot 1 to dot 3 without passing through dot 2 and for quantum information transfer for a double-dot charge qubit.

There are two states orthogonal to the dark state $|D\rangle$: the bright state $|B\rangle = (|1\rangle + |3\rangle)/\sqrt{2}$ and the central state $|C\rangle = |2\rangle$. The 2×2 Hamiltonian matrix spanned by the bright and central states can be analytically diagonalized, and the two eigenstates are expressed as a linear combination of the bright and central state: $|M_1\rangle = \cos(\phi)|B\rangle + \sin(\phi)|C\rangle$ and $|M_2\rangle = -\sin(\phi)|B\rangle + \cos(\phi)|C\rangle$, where $\tan(2\phi) = -\sqrt{2}t/\Delta$. We note that tuning ϕ allows us to recover Jacobi eigenstates discussed in Refs. 17, 24, and 37. Tuning t mostly controls the amount of mixing between the bright and central states in the two eigenstates $|M_1\rangle$ and $|M_2\rangle$, whereas tuning Δ can control the energy spacing between the two eigenstates. The energies associated with the three eigenstates $|D\rangle,|M_1\rangle$, and $|M_2\rangle$ are $E_D = 0$, $E_{M_1} = (\Delta - \Delta_t)/2$, and $E_{M_2} = (\Delta + \Delta_t)/2$ where $\Delta_t = \sqrt{\Delta^2 + 8t^2}$. We note that $|M_1\rangle$ is always the ground state.

Next, we address the two-electron case. The simpler case to analyze is the triplet $S_y = 1$ subspace, which contains two spins up in the LTQD. There are three basis vectors $\{|T_1\rangle, |T_2\rangle, |T_3\rangle\}$, where $|T_1\rangle = \hat{c}^\dagger_{2\uparrow}\hat{c}^\dagger_{1\uparrow}|0\rangle$, $|T_2\rangle = \hat{c}^\dagger_{3\uparrow}\hat{c}^\dagger_{1\uparrow}|0\rangle$, and $|T_3\rangle = \hat{c}^\dagger_{3\uparrow}\hat{c}^\dagger_{2\uparrow}|0\rangle$, respectively. The Hubbard Hamiltonian in this basis reads as

$$H_{2T} = \begin{bmatrix} \Delta + V' & t & 0 \\ t & V & t \\ 0 & t & \Delta + V' \end{bmatrix}. \tag{5}$$

The triplet Hamiltonian [Eq. (5)] and the single-particle Hamiltonian [Eq. (4)] have the identical matrix structure. Therefore, there is a dark triplet eigenstate $|T_D\rangle = (|T_1\rangle - |T_3\rangle)/\sqrt{2}$ and the bright $|T_B\rangle = (|T_1\rangle + |T_3\rangle)/\sqrt{2}$ and central state $|T_C\rangle = |T_2\rangle$. Rotating the Hamiltonian equation (5) into the basis of bright, central, and dark states, a 2×2 Hamiltonian matrix coupling the bright and central states is derived. The two eigenstates of the triplet subspace are $|M_1^T\rangle = \sin(\phi)|T_B\rangle + \cos(\phi)|T_C\rangle$ and $|M_2^T\rangle = -\cos(\phi)|T_B\rangle + \sin(\phi)|T_C\rangle$, where $\tan(2\phi) = \sqrt{2}t/\Delta_v$ and $\Delta_v = \Delta + V' - V$. The corresponding eigenenergies of the three states are

$$E_{T_D} = \Delta + V', \tag{6a}$$

$$E_{M_1^T} = \Delta + V' - \tfrac{1}{2}(\Delta_v + \sqrt{(\Delta_v)^2 + 8t^2}), \tag{6b}$$

$$E_{M_2^T} = \Delta + V' - \tfrac{1}{2}(\Delta_v - \sqrt{(\Delta_v)^2 + 8t^2}). \tag{6c}$$

The ground state $|M_1^T\rangle$ is predominantly characterized by $|T_C\rangle = |\uparrow_1\uparrow_3\rangle$ with spins up in dots 1 and 3 because the corresponding coefficient $\sin(2\phi) \approx 1 - \frac{t^2}{2\Delta_v^2}$ when t/Δ is small. Nevertheless, $|M_1^T\rangle$ still has nonzero presence in both $|T_1\rangle = |\uparrow_1\uparrow_2\rangle$ and $|T_3\rangle = |\uparrow_2\uparrow_3\rangle$ configurations. In later sections, we will explain how the low-bias spin-blockade formation is related to the small yet finite components of $|T_1\rangle$ and $|T_3\rangle$ in $|M_1^T\rangle$ wave function. We designate three ground states in each of the spin-resolved triplet subspaces with $(S = 1, S_y = 1, 0, -1)$ as $|T^+\rangle$, $|T^0\rangle$, and $|T^-\rangle$, respectively. $|T^+\rangle = |M_1^T\rangle$ as was shown above, $|T^0\rangle$ is obtained by flipping one spin and performing symmetrization of the wave function, and $|T^-\rangle$ is obtained by flipping both spins from $|T^+\rangle$. These states will play the major roles in the transport through LTQD at the low source-drain bias. Furthermore, we find it also useful to represent $|T^+\rangle$ as

$$|T^+\rangle = \gamma\left(|T_2\rangle + \frac{\gamma_1}{\gamma}|T_1\rangle + \frac{\gamma_2}{\gamma}|T_3\rangle\right), \tag{7}$$

where the coefficients $|\gamma_{1(2)}| \ll 1$.

Next, we analyze the $S_y = 0$ singlet state for two electrons. We define the following basis: $\{|S_1\rangle, |S_2\rangle, |S_3\rangle, |S_4\rangle, |S_5\rangle, |S_6\rangle\}$. The singly occupied configurations are $|S_1\rangle = \frac{1}{\sqrt{2}}(\hat{c}^\dagger_{1\downarrow}\hat{c}^\dagger_{2\uparrow} + \hat{c}^\dagger_{2\downarrow}\hat{c}^\dagger_{1\uparrow})|0\rangle$, $|S_2\rangle = \frac{1}{\sqrt{2}}(\hat{c}^\dagger_{1\downarrow}\hat{c}^\dagger_{3\uparrow} + \hat{c}^\dagger_{3\downarrow}\hat{c}^\dagger_{1\uparrow})|0\rangle$, and $|S_3\rangle = \frac{1}{\sqrt{2}}(\hat{c}^\dagger_{2\downarrow}\hat{c}^\dagger_{3\uparrow} + \hat{c}^\dagger_{3\downarrow}\hat{c}^\dagger_{2\uparrow})|0\rangle$. The doubly occupied configurations are $|S_4\rangle = \hat{c}^\dagger_{1\downarrow}\hat{c}^\dagger_{1\uparrow}|0\rangle$, $|S_5\rangle = \hat{c}^\dagger_{2\downarrow}\hat{c}^\dagger_{2\uparrow}|0\rangle$, and $|S_6\rangle = \hat{c}^\dagger_{3\downarrow}\hat{c}^\dagger_{3\uparrow}|0\rangle$. The Hubbard Hamiltonian in this basis reads as

$$H_{2S} = \begin{bmatrix} \Delta + V' & t & 0 & \sqrt{2}t & \sqrt{2}t & 0 \\ t & V & t & 0 & 0 & 0 \\ 0 & t & \Delta + V' & 0 & \sqrt{2}t & \sqrt{2}t \\ \sqrt{2}t & 0 & 0 & U & 0 & 0 \\ \sqrt{2}t & 0 & \sqrt{2}t & 0 & 2\Delta + U & 0 \\ 0 & 0 & \sqrt{2}t & 0 & 0 & U \end{bmatrix}. \tag{8}$$

The 3×3 upper left block, spanned by $\{|S_1\rangle, |S_2\rangle, |S_3\rangle\}$, is identical to the triplet Hamiltonian equation (5). For $|\Delta|$ small compared to onsite Coulomb repulsion U, the energy spectrum of the singlet subspace can be divided into the bands of singly occupied and doubly occupied configurations, with a gap of the order of U. Under such a condition, the energies and wave functions of the first three lowest singlet states are very similar to those of the triplet states, and the mixing between singly and doubly occupied configurations leads to a t-J model.[26] However, if $|\Delta|$ is comparable to U, then the singlet subspace has a ground state predominantly characterized by $|S_2\rangle$ configuration, which is well separated from the four excited states characterized by $|S_1\rangle, |S_3\rangle, |S_4\rangle, |S_6\rangle$. The doubly occupied $|S_4\rangle$ and the singly occupied $|S_1\rangle$ configurations, which are connected by tunneling between dots 1 and 2, get very close in energy. When these states are degenerate, two eigenstates can be obtained by $|U_{14}^\pm\rangle = \frac{1}{\sqrt{2}}(|S_1\rangle \pm |S_4\rangle)$. Similarly, we get $|U_{36}^\pm\rangle = \frac{1}{\sqrt{2}}(|S_3\rangle \pm |S_6\rangle)$ from $|S_3\rangle$ and $|S_6\rangle$. By second-order perturbation theory, the well-isolated ground state with dominant contribution from $|S_2\rangle$ has energy

$$E_{M_1^S} = V - 4t^2\left(\frac{1}{\Delta + V' + U - V + 2\sqrt{t}} + \frac{1}{\Delta + V' + U - V - 2\sqrt{t}}\right). \tag{9}$$

We note that the singlet-triplet splitting is $E_{M_1^T} - E_{M_1^S} > 0$ for all range of Δ_v and t, and we have the singlet as the ground state.

Next, we consider the three electron states. In the fully spin polarized subspace, $S_y = +3/2$, there is only one state $|S = 3/2, S_y = +3/2\rangle = \hat{c}^\dagger_{3\uparrow}\hat{c}^\dagger_{2\uparrow}\hat{c}^\dagger_{1\uparrow}|0\rangle$, with energy given by $E^{3/2} = 3E + \Delta + 2V' + V$. This state is characterized by having a spin-up electron in each dot. For $S_y = +1/2$ subspace, it is composed of nine singly and doubly occupied configurations. To simplify the qualitative analysis, we focus on a truncated basis composed of the following three singly occupied configurations: $|a\rangle = \hat{c}^\dagger_{3\uparrow}\hat{c}^\dagger_{2\uparrow}\hat{c}^\dagger_{1\downarrow}|0\rangle$, $|b\rangle = \hat{c}^\dagger_{3\uparrow}\hat{c}^\dagger_{2\downarrow}\hat{c}^\dagger_{1\uparrow}|0\rangle, |c\rangle = \hat{c}^\dagger_{3\downarrow}\hat{c}^\dagger_{2\uparrow}\hat{c}^\dagger_{1\uparrow}|0\rangle$, and two doubly occupied configurations $|d\rangle = \hat{c}^\dagger_{3\uparrow}\hat{c}^\dagger_{1\uparrow}\hat{c}^\dagger_{1\downarrow}|0\rangle$, $|e\rangle = \hat{c}^\dagger_{3\uparrow}\hat{c}^\dagger_{3\downarrow}\hat{c}^\dagger_{1\uparrow}|0\rangle$. Figure 2 shows resonance between configuration $|b\rangle$ and $|e\rangle$ when $|\Delta| = O(U)$. The three-dimensional subspace with singly occupied configurations with $S_y = 1/2$ can be further decomposed by the total spin S, since S is also a good quantum number. For the subspace with $S = 1/2$, we use the Jacobi basis states L_0 and L_1 (Refs. 22 and 23): $|L_0\rangle = \frac{1}{\sqrt{2}}(|a\rangle - |c\rangle)$, $|L_1\rangle = \frac{1}{\sqrt{6}}(|a\rangle - 2|b\rangle + |c\rangle)$. For $|L_0\rangle$, the spin

state in dots 1 and 3 is a singlet. For $|L_1\rangle$, the spin state in dots 1 and 3 can be written as a linear combination of triplets with $S_y = 0$ and $S_y = 1$. The remaining Jacobi state $|L_2\rangle = \frac{1}{\sqrt{3}}(|a\rangle + |b\rangle + |c\rangle)$ is a total spin-3/2 state and is decoupled from all other states. In a similar fashion, we form Jacobi coordinates for the two doubly occupied configurations $|X\rangle = \frac{1}{\sqrt{2}}(|d\rangle + |e\rangle)$ and $|Y\rangle = \frac{1}{\sqrt{2}}(|d\rangle - |e\rangle)$. In the subspace of $S = 1/2$ and $S_y = 1/2$, with basis $\{|L_0\rangle, |X\rangle, |L_1\rangle, |Y\rangle\}$, the three-electron Hamiltonian

$$H_{3\,\mathrm{el}} = \begin{bmatrix} \Delta + 2V' + V & -t & 0 & 0 \\ -t & U + 2V & 0 & 0 \\ 0 & 0 & \Delta + 2V' + V & \sqrt{3}t \\ 0 & 0 & \sqrt{3}t & U + 2V \end{bmatrix} \tag{10}$$

separates into the pair of Hamiltonians describing Jacobi basis states $|L_0\rangle$ and $|L_1\rangle$ entangled with the doubly occupied configurations. Each submatrix can be diagonalized and the eigenstates read as $|L_0^+\rangle = \cos(\phi)|L_0\rangle + \sin(\phi)|X\rangle$, $|L_0^-\rangle = \sin(\phi)|L_0\rangle - \cos(\phi)|X\rangle$, $|L_1^+\rangle = \cos(\theta)|L_1\rangle + \sin(\theta)|Y\rangle$, and $|L_1^-\rangle = \sin(\theta)|L_1\rangle - \cos(\theta)|Y\rangle$, where $\tan(2\phi) = t/\xi$, $\tan(2\theta) = \sqrt{3}t/\xi$, and $\xi = (\Delta + 2V' - U - V)/2$. Here, we observe that each of the two Jacobi states, characterizing the (1,1,1) configuration, hybridizes with both doubly occupied configurations $|X\rangle$ and $|Y\rangle$ to form the eigenstates of a central-dot biased system. All four eigenstates $|L_0^\pm\rangle$ and $|L_1^\pm\rangle$ are current conducting because electrons can be removed from the orbitals in the edge dots to make a transition from the three-electron state to a two-electron (1,0,1) configuration.

In Fig. 3(a), we show the evolution of the five lowest-energy levels of the three-electron complex in the $S_y = 1/2$ subspace as a function of bias Δ in the central dot. At $\Delta = 0$, the spectrum is divided into two bands. The lower band consists of $|L_1\rangle$, $|L_0\rangle$, and $|L_2\rangle$ states, which are all characterized by singly occupied configurations. The upper band consists of states with dominant configurations $|d\rangle$ and $|e\rangle$. As Δ increases, the energy difference between the singly occupied configurations and specific doubly occupied configurations $|d\rangle$ and $|e\rangle$ diminishes. However, the ground state is always the $|L_1^+\rangle$ state in the figure. The blue curve represents the spin-3/2 state, which does not interact with all other levels due to the conservation of total spin of the Hamiltonian. In the plot, the levels are artificially shifted for better visualization. In the inset of Fig. 3(a), the proper energy levels around the anticrossing point are shown in detail. Figure 3(b) shows the configuration content of the ground state as a function of bias Δ. At $\Delta = 0$, the ground state is dominated by singly occupied configuration $|L_1\rangle$, but at higher bias $\Delta \approx U$, the doubly occupied configuration $|Y\rangle$ reaches around 50% content of the ground state.

B. Current through a linear triple quantum dot

The theory of sequential tunneling through a triangular TQD molecule has been described in detail in Ref. 20. Here, we extend the approach to include both electron-phonon interaction and cotunneling and apply this theory to describe

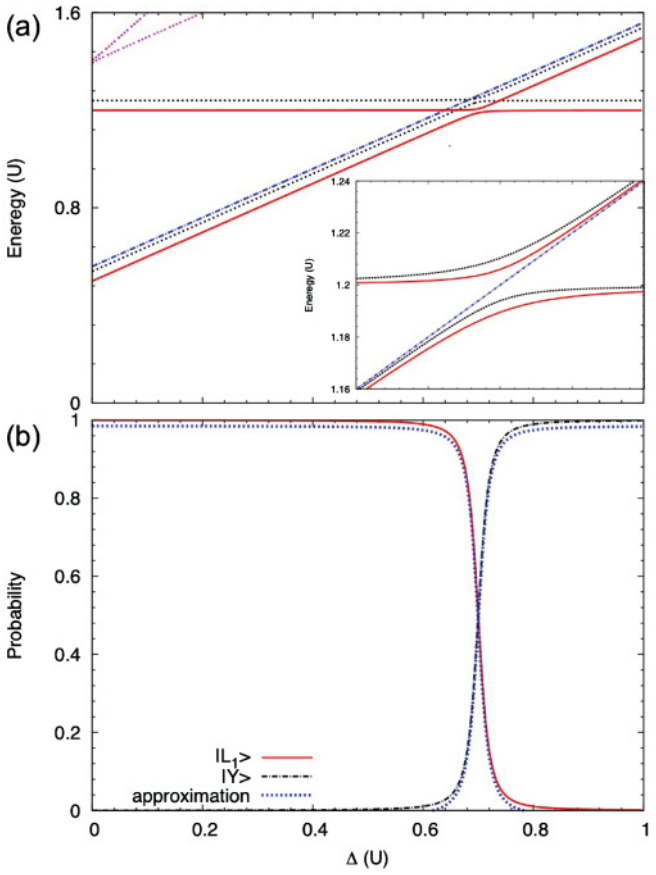

FIG. 3. (Color online) (a) The three-electron molecule energy spectrum with total $S_y = 1/2$ as a function of bias Δ, obtained from the single-band Hubbard model. As Δ increases, the five energy levels anticross. The blue curve, corresponding to total spin-3/2 state, does not interact with the other states. The energy levels are artificially shifted by a constant values for better visibility. The inset shows the energy levels near the anticrossing point. (b) Shows the projection of the ground state onto $|L_1\rangle$ (the red curve) and $|Y\rangle$ (the black curve) states. The wave function of the ground state is obtained from exact diagonalization of the single-band Hubbard model. The blue dashed lines provide the same information but obtained from the analytical approximation for $|L_1^+\rangle = \cos(\theta)\,|L_1\rangle + \sin(\theta)\,|Y\rangle$ discussed in the text.

current and spin blockade in a LTQD. Following Refs. 20, 38, 43, and 44, the current between lead r and a TQD device in the vicinity of a QP involving $N = 2$ and $N + 1 = 3$ electrons can be written as a difference between the current from the lead to the TQD and a current from the TQD back to the lead r:

$$I_{rD} = -e \sum_{i_r,\sigma} \sum_{\alpha_N,\beta_{N+1}} W_r^{\mathrm{seq}}(\alpha_N \to \beta_{N+1}) P_{\alpha_N} + e \sum_{i_r,\sigma} \sum_{\alpha_N,\beta_{N+1}} W_r^{\mathrm{seq}}(\beta_{N+1} \to \alpha_N) P_{\beta_{N+1}}, \tag{11}$$

where $|\alpha_N\rangle$ is an N-electron many-body eigenstate of the isolated TQD with energy E_{α_N} and associated steady-state probability P_{α_N}, obtained by solving the rate equation as explained below. The sequential tunneling rate $W_r^{\mathrm{seq}}(\alpha_N \to \beta_{N+1})$ provides the rate of transition for the TQD from

an N-electron α_N state to an $(N+1)$-electron state due to first-order perturbation from the lead r. Details of sequential tunneling rates will be provided later.

The probabilities P_{α_N}'s are the diagonal matrix elements of the reduced density matrix ρ. The time evolution of these diagonal matrix elements is described by the Pauli master equation

$$\dot{P}_{\alpha_N} = \sum_{N'=2}^{3} \sum_{\beta_{N'}} P_{\beta_{N'}} W(\beta_{N'} \to \alpha_N) - P_{\alpha_N} W(\alpha_N \to \beta_{N'}), \tag{12}$$

where transition rates $W_{\alpha_N \to \beta_{N'}}$ are calculated using Fermi's golden rule. We consider sequential tunneling rate $W_r^{\rm seq}$ in first order in coupling to the lead r, intra-TQD phonon-induced relaxation rate W^{ph}, and second-order cotunneling rate $W_r^{\rm cot}$. The master equation is solved to obtain steady-state solution for the probabilities P_{α_N} by setting the time derivatives to be zero.

With the coupling to a lead r in Eq. (2), the first-order sequential tunneling rates read as

$$W_r^{\rm seq}(\alpha_N \to \beta_{N+1}) = \frac{2\pi}{\hbar} \sum_k \left| \langle \beta_{N+1} | \sum_i \tilde{t}_i^r(k) \hat{c}_{i\sigma}^\dagger | \alpha_N \rangle \right|^2 \times \delta(\omega_{\alpha\beta} - \epsilon_{rk}) f_r(\omega_{\alpha\beta}), \tag{13a}$$

$$W_r^{\rm seq}(\beta_{N+1} \to \alpha_N) = \frac{2\pi}{\hbar} \sum_k \left| \langle \alpha_N | \sum_i \tilde{t}_i^r(k) \hat{c}_{i\sigma} | \beta_{N+1} \rangle \right|^2 \times \delta(\omega_{\alpha\beta} - \epsilon_{rk})(1 - f_r(\omega_{\alpha\beta})), \tag{13b}$$

where $f_r(\epsilon) = 1/\{\exp[(\epsilon - \mu_r)/k_B T] + 1\}$ is the Fermi function of the lead r, $\omega_{\alpha\beta} = E_{\beta_{N+1}} - E_{\alpha_N}$, and ϵ_{rk} is the energy of a state associated with wave vector k of lead r. We remark that the summation over index i in the sequential tunneling rate refers to summing the tunneling contributions from the S and P orbitals in a quantum dot. By expanding the norms of the complex-valued matrix elements in the above equations and introducing an integration variable ω, the sequential tunneling rates can be also expressed as follows:

$$W_r^{\rm seq}(\alpha_N \to \beta_{N+1}) = \frac{2\pi}{\hbar} \sum_{i,j} \int d\omega A_{ij}^{\alpha\beta}(\omega) B_{ij}^r(\omega) f_r(\omega_{\alpha\beta}), \tag{14a}$$

$$W_r^{\rm seq}(\beta_{N+1} \to \alpha_N) = \frac{2\pi}{\hbar} \sum_{i,j} \int d\omega A_{ij}^{\alpha\beta}(\omega) B_{ij}^r(\omega)[1 - f_r(\omega_{\alpha\beta})], \tag{14b}$$

with generalized spectral functions[45] of the TQD, $A_{ij}^{\alpha\beta} = \sum_\sigma \langle \alpha_N | \hat{c}_{i\sigma} | \beta_{N+1} \rangle \langle \beta_{N+1} | \hat{c}_{j\sigma}^\dagger | \alpha_N \rangle \delta(\omega - \omega_{\alpha\beta})$, and generalized spectral function of the lead r, $B_{ij}^r(\omega) = \sum_k \tilde{t}_i^r(k)[\tilde{t}_j^r(k)]^* \delta(\omega - \epsilon_{rk})$. By substituting the sequential tunneling rates in Eq. (11) with Eq. (14), one can relate the current through a TQD with the spectral functions of the TQD and the leads.

We now provide relaxation rates due to electron-phonon interaction and cotunneling. For large source-drain bias voltage $|eV_{sd}| \gg |t_{ij}|$, the change in the onsite energy of dots due to the source-drain bias will take the system off the resonance, away from the QP. In this regime, the current is dominated by inelastic tunneling between orbitals of neighboring quantum dots due to electron-phonon interaction. The phonon emission-induced relaxation rate[40] reads as

$$W^{ph}(\alpha_N \to \beta_N) = \frac{2\pi}{\hbar} \sum_{\mathbf{q}} \left| \sum_{i,j,\sigma} M_{ij}(\mathbf{q}) \langle \beta_N | \hat{c}_{i\sigma} \hat{c}_{j\sigma}^\dagger | \alpha_N \rangle \right|^2 \times \delta\left(E_{\alpha_N} - E_{\beta_N} - \hbar\omega_{\mathbf{q}}\right) g(\hbar\omega_{\mathbf{q}}, T), \tag{15}$$

where $\hbar\omega_{\mathbf{q}} = \hbar c_s |\mathbf{q}|$ is phonon energy and $g(\hbar\omega_{\mathbf{q}})$ is the thermal occupation number for phonon mode $\mathbf{q}$ at temperature T. Spin blockade occurs when the spin-3/2 polarized states $|\alpha_3\rangle$ become a trap state, with $W_r^{\rm seq}(\alpha_3 \to \beta_2) = 0$. However, the spin blockade can be lifted if we allow cotunneling. We consider the inelastic cotunneling transition rate,[43,46] which involves an exchange of electrons between a lead r and the TQD in a spin-3/2 state:

$$W_r^{\rm cot}(\alpha_3 \to \beta_3) = \frac{2\pi}{\hbar} \sum_{\sigma,\sigma',k,k'} f_r\left(\epsilon_{k_r'}^{\sigma'}/\hbar\right)\left[1 - f_r\left(\epsilon_{k_r}^{\sigma}/\hbar\right)\right] \delta\left(E_{\beta_3} - E_{\alpha_3} + \epsilon_{k_r}^{\sigma} - \epsilon_{k_r'}^{\sigma'}\right) \left| \sum_{\gamma_2,i,i'} t_i^r(k_r) t_{i'}^r(k_{r'}') \frac{\left(C_{\alpha_3\gamma_2}^{i_r'\sigma'}\right)^* C_{\beta_3\gamma_2}^{i_r\sigma}}{E_{\alpha_3} - E_{\gamma_2} - \epsilon_{k_r}^{\sigma}} \right|^2, \tag{16}$$

where $C_{\alpha_3,\gamma_2}^{i\sigma} = \langle \alpha_3 | \hat{c}_{i\sigma}^\dagger | \gamma_2 \rangle$, $|\gamma_2\rangle$ is a triplet state, and $\epsilon_{k_r}^{\sigma}$ is the energy for an electron with wave vector k and spin σ of the lead r. In Eq. (16), we have considered only inelastic contribution of the cotunneling rate, as the resonant cotunneling rate[47] is exponentially suppressed at the low-temperature limit.

III. TRANSPORT AND SPIN BLOCKADE

In this section, we compute and discuss the transport properties and spin blockade in a LTQD at both SQP and AQP. We set onsite Coulomb repulsion between S orbitals to be $U_{11} = U_{22} = U_{33} = U = 3.0$ meV, and we use U as the unit of energy scale. For S and P orbitals in the same dot, we set $U_{14} = U_{35} = U' = 0.94U$, and $U_{44} = U_{55} = U'' = 0.96U$ for P orbitals in the same dot. We set $t_{i,j} = t = -6.0 \times 10^{-3}\, U$ for tunneling between S orbitals in neighboring dots. We set $t_{ij} = t' = -6.2 \times 10^{-3}\, U$ for tunneling between the S and P orbitals on neighboring dots. We set $V_{ij} = V' = 0.2\, U$ between neighboring dots and $V_{ij} = V = 0.1\, U$ between dots 1 and 3. The energy difference between S and P energy levels Δ_{sp} in the same dot is taken to be $0.8U$ and $0.25U$ in different cases considered below.

The tunnel coupling for the tight-binding chain in the leads is taken as $t_L = t_R = -2.0U$. The large tunnel coupling

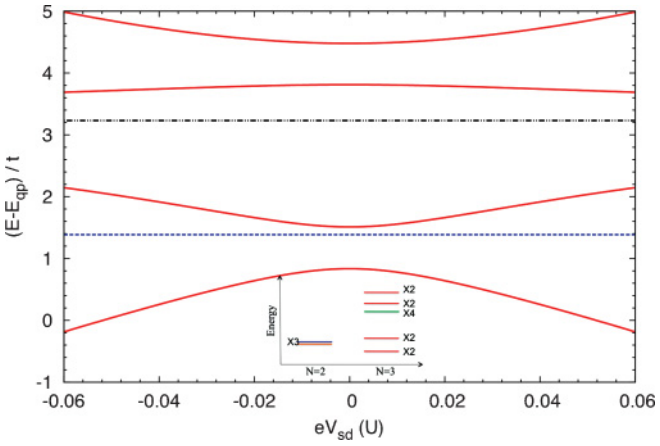

FIG. 4. (Color online) The energy spectrum of a multiband Hubbard model as a function of source-drain bias. In the figure, the blue curve represents the four two-electron states. They are very close in energy and look degenerate in the energy resolution present here. The green curve is the quadruply degenerate spin-3/2 states. The red curves are each doubly degenerate spin-1/2 states. Inset: A summary of the states involved in the main figure at a particular value of V_{sd}.

for the leads allows a wide energy band, which increases the amount of available states for transport. As for the dot-lead tunnel coupling t_i^r, we set $t_1^L = -1.0 \times 10^{-3} U$ and $t_4^L = -1.1 \times 10^{-3} U$. Only the S and P orbital in dot 1 is connected to the left lead. Symmetrically, we set $t_3^R = t_1^L$ and $t_5^R = t_4^L$. The rest of the tunnel coupling parameters are zero in our model. For interaction between electrons in the TQD and bulk LA phonons, we use the following GaAs parameters: $\Lambda(q) = \sqrt{D^2 \hbar \omega_q / 2\rho c_s^2}$, where $D = 2.9\,U$, $\rho = 5300$ kg/m^3, $c_s = 3700$ m/s, and $\omega_q = c_s q$.

We measure current in unit of $I_0 = e|t_1^L|^2/\hbar|t_L|$. We assume total potential difference eV_{sd} across the two leads and a linear decrease of this potential across the device. The chemical potentials on the two leads are given by $\mu_L = eV_{sd}/2$ and $\mu_R = -eV_{sd}/2$. The onsite energies are given by $E_{1,(4)}(V_{sd}) = E^0_{1,(4)} + eV_{sd}/6$, $E_{i_2} = E^0_{i_2}$, and $E_{3,(5)}(V_{sd}) = E^0_{3,(5)} - eV_{sd}/6$, respectively, and electron temperature in all calculations is set to $k_B T = 2.0 \times 10^{-3}\,U$.

A. Quantum-interference-based spin blockade

We first consider transport through the SQP: {(1,0,1), (2,0,1), (1,1,1), (1,0,2)}, and we assume that the quantum dot potentials are tuned in such a way that the P orbitals ($i = 4,5$) in edge dots may participate in the electronic transport. We set $E_1 = E_3 = -U - V$ and $E_2 = -2V'$ in order to bring the four charge configurations into resonance. For the present case, we set a high single-particle level spacing $\Delta_{SP} = 0.8U$ in the edge dots. A large energy spacing between the S and P orbitals allows one to focus on a few lowest states for transport at bias $|eV_{sd}| \ll U$. For instance, Fig. 4 shows the energy diagrams of the relevant two- and three-electron states near the SQP as a function of V_{sd}. In the presence of small V_{sd}, the energy spectrum does not alter much and the wave functions remain similar to the wave functions at zero V_{sd}. The inset in Fig. 4 categorizes the states associated with the energies in the main figure. There are four active two-electron states: one singlet $|S\rangle$, and triply degenerate triplet states $|T^{\pm,0}\rangle$. These four states are characterized predominantly by the (1,0,1) charge configurations as discussed in Sec. II A. For $N = 3$ subspace, there are four spin-1/2 states below the spin-3/2 states. The four spin-1/2 states are $|L_1^+\rangle$ and $|L_0^+\rangle$ and their counterpart in the $S_y = -1/2$ subspace. In the absence of magnetic field, these states remain degenerate. Next up in the three-electron subspace are the quadruply degenerate spin-3/2 states $|S = 3/2, S_y = \pm 1/2, \pm 3/2\rangle$. The last four levels are $|L_1^-\rangle$ and $|L_0^-\rangle$ states and their counterpart in $S_y = -1/2$ subspace. We emphasize that these three-electron states are admixtures of (2,0,1), (1,1,1), and (1,0,2) configurations with comparable weights except the spin-polarized states as discussed in Sec. II A. Based on the analysis of wave functions, obtained from the exact diagonalization of a single-band Hubbard Hamiltonian, the only dark channels[38] in the LTQD are the spin-3/2 states. As the spin-3/2 wave functions $|S = 3/2, S_y = \pm 1/2, \pm 3/2\rangle$ do not overlap significantly with the two-electron triplet states $|T^{\pm,0}\rangle$, when an electron is added or removed from the edge dots, the conventional spin blockade is not expected in this regime.

Figure 5(a) shows the current $I(V_{sd})$ of a LTQD and Fig. 5(b) shows the steady-state occupation probability of the four spin-3/2 states as functions of V_{sd}. This was done by setting the cotunneling rate $W^r_{\rm cot} = 0$. The I-V_{sd} curve is symmetrical with respect to the bias direction as it should be at SQP. The most prominent feature is that the vanishing of the current and therefore significant negative differential conductance associated with high occupation probability of the spin-3/2 states. As shown in Fig. 5(a), the current is completely suppressed at a very limited bias regime; this is very different from the I-V curve in the spin-blockade regime in a DQD. These numerical results are obtained from a five-level Hubbard model, and the negative differential conductance is not reproduced when we use just the three-level Hubbard model for the transport calculation. This implies that this negative differential conductance is related to the existence of the high-energy P orbitals.

In order to explain this negative differential conductance, we need to study $S_y = 3/2$ subspace with all five orbitals. There are 10 possible configurations for three spin-up electrons in five orbitals. Using the Hubbard model with these five orbitals, the configuration with the lowest energy is $|\uparrow_1, \uparrow_2, \uparrow_3\rangle = \hat{c}^\dagger_{1\uparrow}\hat{c}^\dagger_{2\uparrow}\hat{c}^\dagger_{3\uparrow}|0\rangle$, and the next two configurations are $|\uparrow_1, \uparrow_3, \uparrow_5\rangle = \hat{c}^\dagger_{1\uparrow}\hat{c}^\dagger_{3\uparrow}\hat{c}^\dagger_{5\uparrow}|0\rangle$ and $|\uparrow_1, \uparrow_3, \uparrow_4\rangle = \hat{c}^\dagger_{1\uparrow}\hat{c}^\dagger_{3\uparrow}\hat{c}^\dagger_{4\uparrow}|0\rangle$. Configuration $|\uparrow_1, \uparrow_2, \uparrow_3\rangle$ is separated from $|\uparrow_1, \uparrow_3, \uparrow_5\rangle$ and $|\uparrow_1, \uparrow_3, \uparrow_4\rangle$ by an energy gap of $\sim U + \Delta_{sp} - \Delta$. The other seven configurations are even further away in energy. The Hamiltonian of this low-energy configuration subspace in the basis of $\{|\uparrow_1, \uparrow_3, \uparrow_5\rangle, |\uparrow_1, \uparrow_2, \uparrow_3\rangle, |\uparrow_1, \uparrow_3, \uparrow_4\rangle\}$ is

$$H_{3/2} = \begin{bmatrix} E_1 + 2E_3 + \Delta_{sp} + U' + 2V & -t' & 0 \\ -t' & E_1 + E_2 + E_3 + 2V' + V & -t' \\ 0 & -t' & 2E_1 + E_3 + \Delta_{sp} + U' + 2V \end{bmatrix}, \quad (17)$$

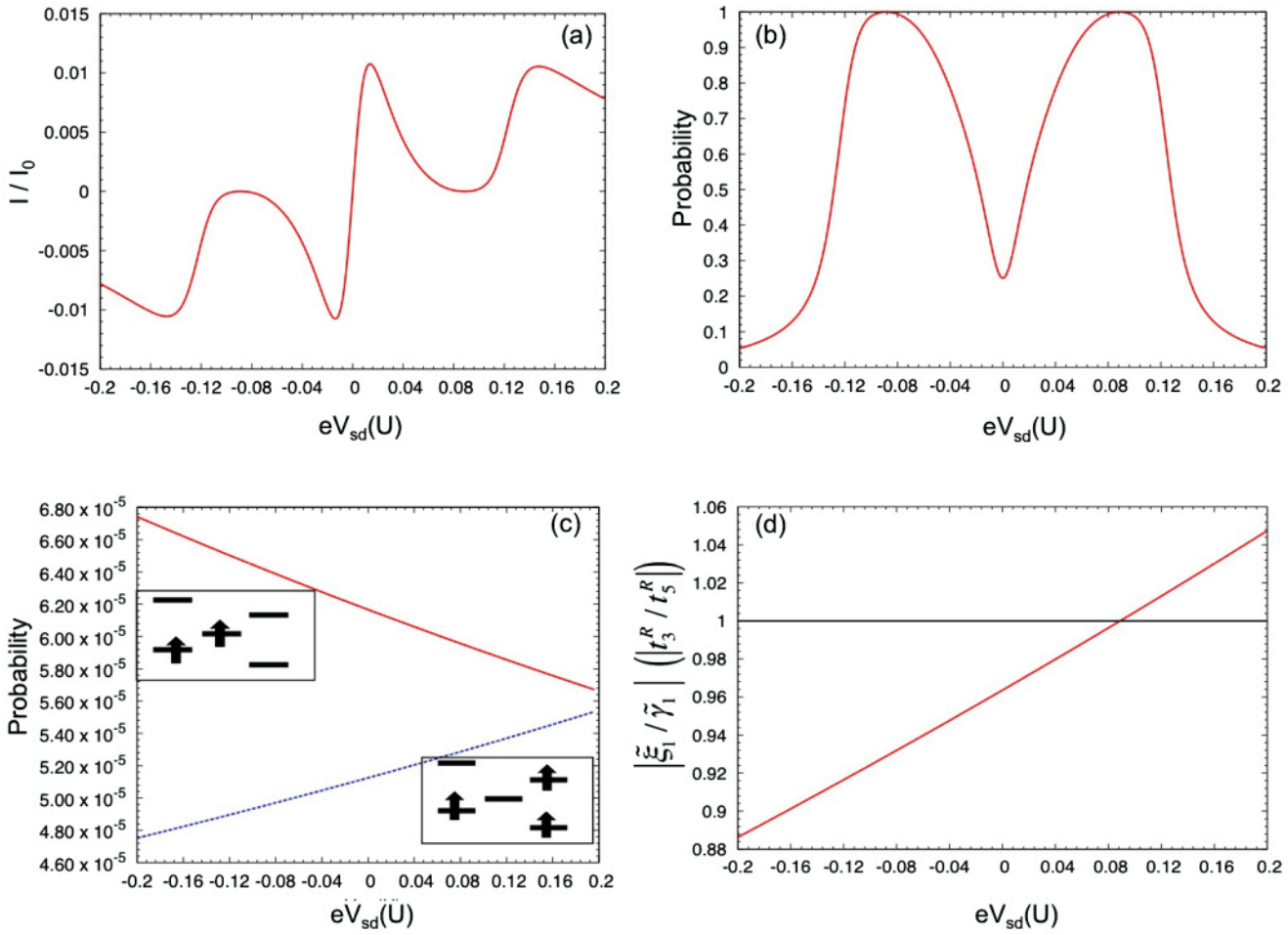

FIG. 5. (Color online) (a) The current $I(V_{sd})$ as function of the applied source-drain bias V_{sd} of a LTQD at the SQP in the low source-drain bias regime. Note zero current at $V_{sd} \approx \pm 0.08$. (b) The steady-state occupation probability of the spin-3/2 states as a function of V_{sd}. Panels (a) and (b) together indicate that the spin-3/2 states are related to the bidirectional, quantum-interference-based dark channel in a LTQD. (c) Projection of the triplet state $|T^+\rangle$ onto the configuration $\hat{c}^\dagger_{1\uparrow}\hat{c}^\dagger_{2\uparrow}|0\rangle$, and the projection of the spin-3/2 state $|3/2\rangle$ onto the configuration $\hat{c}^\dagger_{1\uparrow}\hat{c}^\dagger_{3\uparrow}\hat{c}^\dagger_{5\uparrow}|0\rangle$. (d) Ratio of matrix elements $|\frac{\eta_1}{\gamma_1}|$ (see text for the definition) in the unit of the ratio $|\frac{t_3^R}{t_5^R}|$. Spin blockade is formed when the red curve intercepts $y = 1$ line in the figure. Panels (c) and (d) are presented to illustrate the formation of the spin blockade in the positive bias direction.

where E_1 and E_3 are almost identical when V_{sd} is small. This Hamiltonian matrix looks similar to the two-electron triplet Hamiltonian [Eq. (5)], except that the tunneling matrix elements acquire a negative sign for the three electron system. This negative sign is simply due to the anticommutation relation between fermionic operators. Exact diagonalization of the above Hamiltonian gives a ground state

$$|3/2\rangle = \eta\left(|\Uparrow_1,\uparrow_2,\uparrow_3\rangle + \frac{\eta_1}{\eta}\,|\Uparrow_1,\uparrow_3,\uparrow_5\rangle + \frac{\eta_2}{\eta}\,|\Uparrow_1,\uparrow_3,\uparrow_4\rangle\right), \tag{18}$$

where coefficients $\eta_{1(2)}$ are of the same order of magnitude as the coefficients $\gamma_{1(2)}$ for $|T^+\rangle$ in Eq. (7). This can be understood by analyzing the Hamiltonians. The energy difference between the configurations $|T_1\rangle$ and $|T_3\rangle$ is given by $|\Delta + V' - V|$, and the energy difference between the configurations $|\Uparrow_1,\uparrow_3,\uparrow_5\rangle$ and $|\Uparrow_1,\uparrow_2,\uparrow_3\rangle$ is given by $|\Delta - \Delta_{sp} - U' - V + 2V'|$. Considering that Δ and Δ_{sp} are both of the order of U, the two energy gaps are actually comparable. In general, hybridization of configurations $|i\rangle$ and $|j\rangle$ in a wave function can be estimated by $\frac{\langle i|H|j\rangle}{E_i - E_j}$. In our case, the S-P tunnel coupling t' is of the same order of magnitude as the S-S tunnel coupling t. This explains why $\eta_{1(2)}$ are comparable to $\gamma_{1(2)}$ in magnitude. Furthermore, $\eta_{1(2)}$ have opposite signs with respect to $\gamma_{1(2)}$ because the off-diagonal matrix elements in Eqs. (17) and (5) have opposite signs. Figure 5(c) presents the norm of γ_1 and η_1 from the exact diagonalization of the five-level Hubbard model as a function of V_{sd}.

Next, we look at the rate equation for the state $|3/2\rangle$ when the system is subject to a positive source-drain bias, i.e.,

charging electron from left dot and removing electron from right dot:

$$\frac{dP_{3/2}}{dt} = -W_R^{\rm seq}(3/2 \to T^+)P_{3/2} + W_L^{\rm seq}(T^+ \to 3/2)P_{T^+}. \tag{19}$$

Note that the only allowed two-electron state is $|T^+\rangle$ because the total spin can not change by more than 1/2 when adding an electron. The phonon relaxation does not play a role here because $|3/2\rangle$ and $|T^+\rangle$ are the lowest-energy states in their own spin-resolved subspaces, respectively. For simplicity, we have ignored the cotunneling contribution in this analysis, and numerical results in Fig. 5 are also obtained without the cotunneling terms. Cotunneling effects will be discussed below. In order for $|3/2\rangle$ to be a trap state, the incoming rate $W_L^{\rm seq}(T^+ \to 3/2)$ should dominate over the outgoing rate $W_R^{\rm seq}(3/2 \to T^+)$:

$$\begin{aligned} W_R^{\rm seq}(3/2 \to T^+) &= \frac{2\pi}{\hbar}\sum_k \left|\langle T^+|\tilde{t}_3^R(k)\hat{c}_{3\uparrow}|3/2\rangle + \langle T^+|\tilde{t}_5^R(k)\hat{c}_{5\uparrow}|3/2\rangle\right|^2 \delta(E_{3/2} - E_{T^+} - \epsilon_{kR})(1-f_R), \\ &= \frac{2\pi}{\hbar}\sum_k \left|\left(|\gamma_1|t_3^R - |\eta_1|t_5^R\right)\frac{e^{-ika}}{\sqrt{2\pi}}\right|^2 \delta(E_{3/2} - E_{T^+} - \epsilon_{kR})(1-f_R), \end{aligned} \tag{20}$$

where $\tilde{t}_i^R(k) = t_i^R e^{-ika}/\sqrt{2\pi}$ and f_R is the Fermi function for the right lead. The coefficients γ_1 and η_1 are defined in Eqs. (7) and (18), respectively. The expression $(|\gamma_1|t_3^R - |\eta_1|t_5^R)$ gives the interference between the two possible paths of removing an electron (via the S and P orbitals) from the right dot. The minus sign in the expression stems from the fact that η_1 and γ_1 have opposite signs, and the origin of this sign difference was already explained immediately following Eq. (17). We see that the condition for the quenching of $W_R^{\rm seq}(3/2 \to T^+)$ is $|\gamma_1/\eta_1| = |t_5^R/t_3^R|$. Figure 5(d) presents the ratio $|\gamma_1/\eta_1|$ as a function of V_{sd}. At points of strongest current suppression, we observe that the ratio indeed matches the ratio of $|t_5^R/t_3^R|$. In short, the negative differential conductance sets in whenever the two possible paths (removing an electron from the S or P orbital) of electronic transport become comparable in amplitude and interfere destructively. This destructive interference is possible only for the transport channels through spin-3/2 states. In terms of spin configurations, the transport channel $|3/2\rangle \to |T^+\rangle$ involves the two paths $(\uparrow_1, \uparrow_2, \uparrow_3) \to (\uparrow_1, \uparrow_2)$ and $(\uparrow_1, \uparrow_3, \uparrow_5) \to (\uparrow_1, \uparrow_3)$, which can destructively interfere. For all other transport channels, electronic transport occurs with much higher probability amplitude via the S orbital in the edge dots at the low source-drain bias.

Figures 6(a) and 6(b) show the current through the LTQD and the steady-state probability distribution for the spin-3/2 states in the parameter space of $(E_1 = E_3, E_2)$ at a small bias $eV_{sd} = 0.01\ U$, respectively. In this calculation, the cotunneling effect is included. Although the quantum-interference-based spin blockade is formed under a very specific condition, Fig. 6(b) shows that the interference-based spin blockade can still be observed in the parameter space of onsite energies. The cotunneling effects can be analyzed when we add terms $\sum_{r=L,R}\sum_{\beta_3} W_r^{\rm cot}(\beta_3 \to 3/2)P^{\beta_3} - \sum_{r=L,R}\sum_{\beta_3} W_r^{\rm cot}(3/2 \to \beta_3)P^{3/2}$, where $|\beta_3\rangle$ is a three-electron state with $S = 1/2$, in Eq. (19). In Eq. (20), we analyze the condition for the transition rate from $|3/2\rangle$ to $|T^+\rangle$ to vanish. With cotunneling included in the model, we should analyze the condition for the transition rate from $|3/2\rangle$ to each $|\beta_3\rangle$ state to vanish. In principle, each transport channel has its unique condition for the quenching, and the interference-based quantum spin blockade will be lifted. However, the additional rates due to cotunneling are much smaller in amplitude as they scale with $|t_1^L|^4$ for the second-order processes. The system still gets blockaded in the spin-3/2 state when the sequential tunneling driven transition $[W_R^{\rm seq}(3/2 \to T^+)]$ vanishes because the incoming rate $W_L^{\rm seq}(T^+ \to 3/2)$, a first-order process, scales with $|t_1^L|^2$ and is around five orders of magnitude larger than the rates driven by the cotunneling processes.

Finally, we remark that similar orbital interference-based blockade has recently been reported by Donarini *et al.*[48] for a triangular TQD with one orbital each in the single-electron regime. In the triangular arrangements, the rotational symmetry yields many-body spectrum with degeneracies. Thus, the tunneling electron can travel through two energetically degenerate transport channels to achieve the destructive interference necessary for the blocking state. In this study with a linear TQD, the energetically equivalent paths needed for quantum interference come from the removal or addition of electron via either the S or P orbital in the edge dots as already discussed.

B. Symmetrical and asymmetrical spin blockade

Next, we look at the SQP again with a different single-particle level spacing $\Delta_{sp} = 0.25U$. In this case, we will consider a wider range of source-drain bias with $eV_{sd} > U$. Figure 7(a) shows the current $I(V_{sd})$ of the TQD near the SQP. We again have a symmetric $I(V_{sd})$ with respect to the bias directions and, therefore, the observed negative differential conductance is also bidirectional. We will focus on the positive bias direction for the following discussion. We note that there are two regions where the current is strongly suppressed in the positive bias direction in Fig. 7(a). One point is at the low bias regime $eV_{sd} \ll U$, and the other point is at the high bias regime such that onsite triplet occupation is allowed in the transport window. From Fig. 7(b), we see that the system is trapped in (1,1,1) spin-3/2 states whenever the current is significantly suppressed in Fig. 7(a). The strong current suppression at the low bias is due to the quantum-interference-based spin

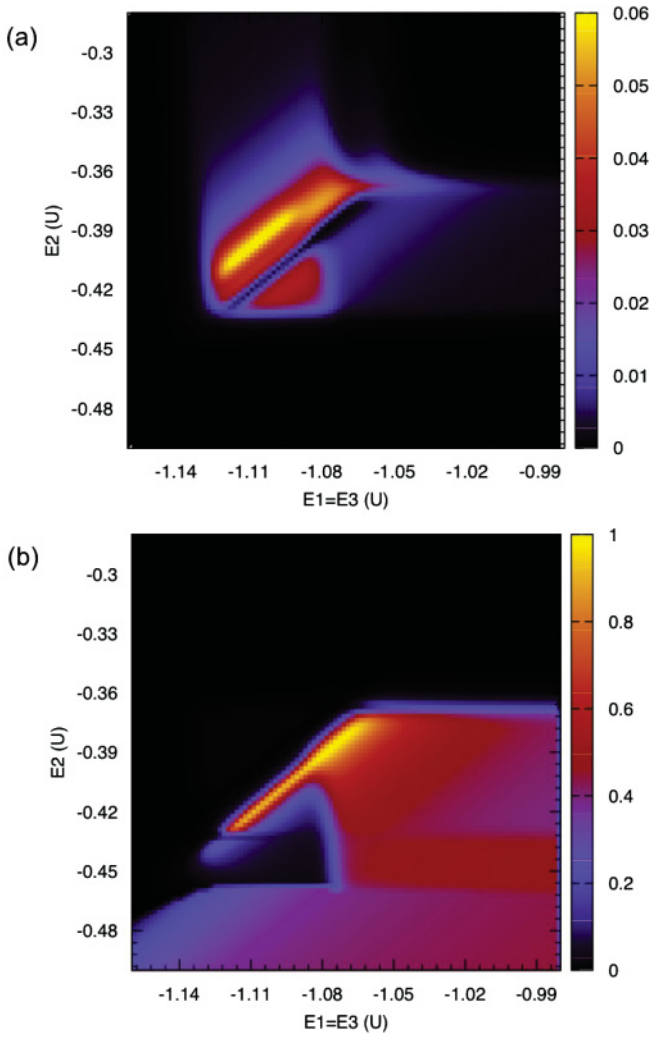

FIG. 6. (Color online) (a) Current of the LTQD in the parameter space of $(E_1 = E_3, E_2)$. The transport region manifests a rounded boundary, which indicates the states involves in the electronic transport are highly hybridized states. The transport region is separated into two parts by a thin line of strong current suppression. This is the region of dark channels. (b) The steady-state occupation probability for spin-3/2 states. High amount of spin-3/2 states are found exactly where the currents vanish in panel (a).

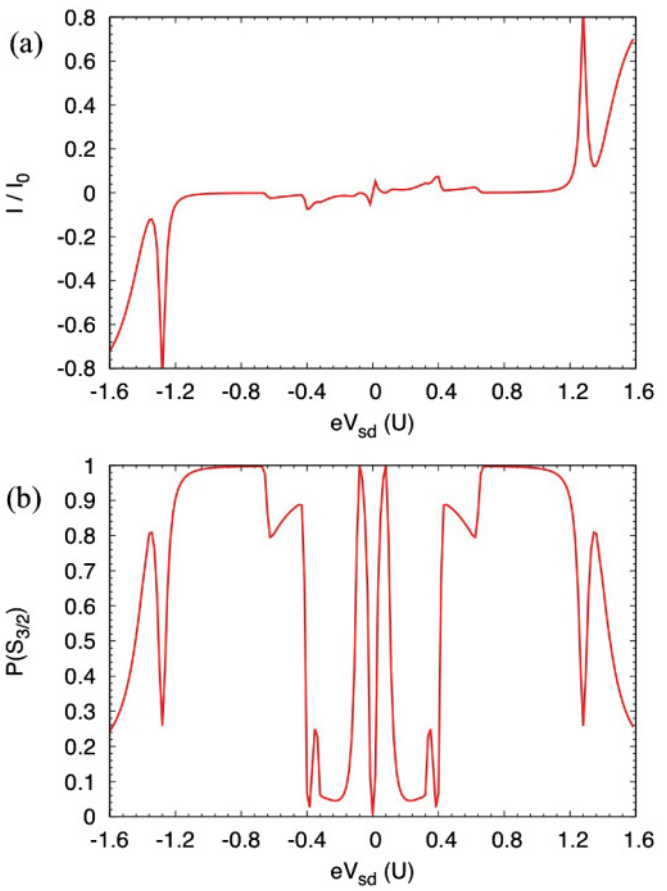

FIG. 7. (Color online) (a) Current of the LTQD at the SQP as a function of eV_{sd}. In both bias directions, we observe negative differential conductances at two different bias regimes. (b) The steady-state occupation probability for spin-3/2 states. The two panels together show that the LTQD is trapped in spin-3/2 state whenever the current is strongly suppressed.

blockade we described in the previous section. As source-drain bias is further increased, the wave function inside the LTQD also changes. Gradually one path of electronic transport becomes preferred and quantum interference vanishes. At the high bias, the second current suppression is identified to be the more familiar spin-blockade phenomenon in the double quantum dot, and it is characterized by an extended region of current suppression over a wider range of source-drain bias. At high bias, hybridization of levels becomes insignificant, and it is instructive to look at each eigenstate as a particular localized configuration. Figure 8 presents a schematics of how this high-bias spin blockade is formed and lifted in the LTQD at high bias. The spin blockade is formed when the onsite triplet becomes accessible in the left dot but not in the right dot in the transport window when a positive bias is applied. Due to the phonon-induced relaxation, the onsite triplet in the left dot will relax by allowing electron-phonon scattering to redistribute the electron from the P orbital in the edge dot onto the S orbital in the central dot. When the onsite triplet state in the right dot is still too high in energy for occupation, the system gets stuck in this $(1,1,1)$ spin-3/2 configuration. This spin blockade is lifted when the bias is further increased so the onsite triplet becomes accessible in the right dot too. Then, the phonon-induced relaxation will again help transfer the electron from the central dot onto the right dot. We remark that the spin blockade does not happen in this model if the phonon-induced relaxation mechanism is removed. From this picture, we can derive the spin-blockade regime from the parameters we used. The energies of the relevant configurations are

$$\begin{aligned} E(\uparrow_1\uparrow_3) &= E_1 + E_3 + V = -2.1U, \\ E(\uparrow_1\uparrow_3\uparrow_4) &= 2E_1 + \Delta_{sp} + E_3 + U' + 2V + \frac{eV_{sd}}{6} \\ &= -1.91U + \frac{eV_{sd}}{6}, \\ E(\uparrow_1\uparrow_2\uparrow_3) &= E_1 + E_2 + E_3 + 2V + V' = -2.1U, \\ E(\uparrow_1\uparrow_3\uparrow_5) &= E_1 + 2E_3 + \Delta_{sp} + U' + 2V - \frac{eV_{sd}}{6} \\ &= -1.91U - \frac{eV_{sd}}{6}. \end{aligned}$$

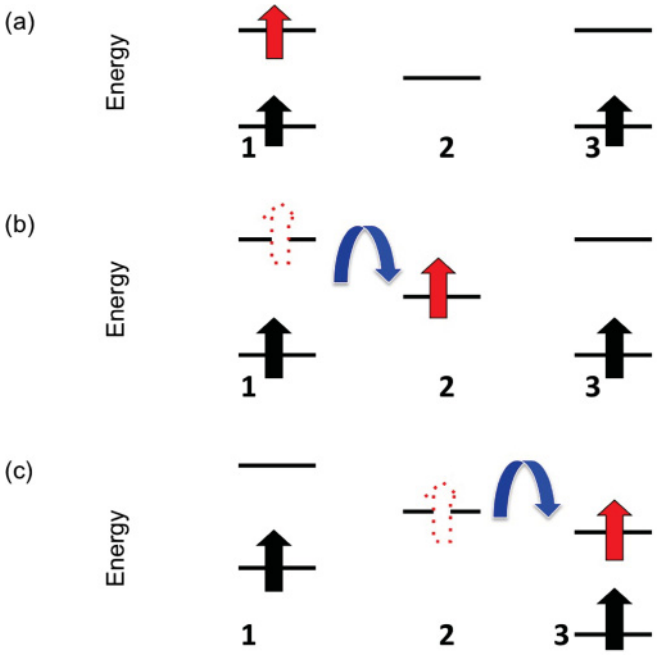

FIG. 8. (Color online) Schematic representation of lifting of spin blockade. (a) (2,0,1) configuration obtained from the (1,0,1) configuration when an additional electron tunnels onto the P orbital of dot 1. (b) Due to phonon-induced relaxation in the model, the added spin moves from the P orbital in dot 1 to the S orbital in dot 2. However, it does not proceed further to the dot 3 because this costs energy. (c) At larger source-drain bias in the positive direction, the energy levels in dot 3 are lowered with respect to those of dot 2. Thus, the phonon-induced relaxation assists the electron to move onto dot 3.

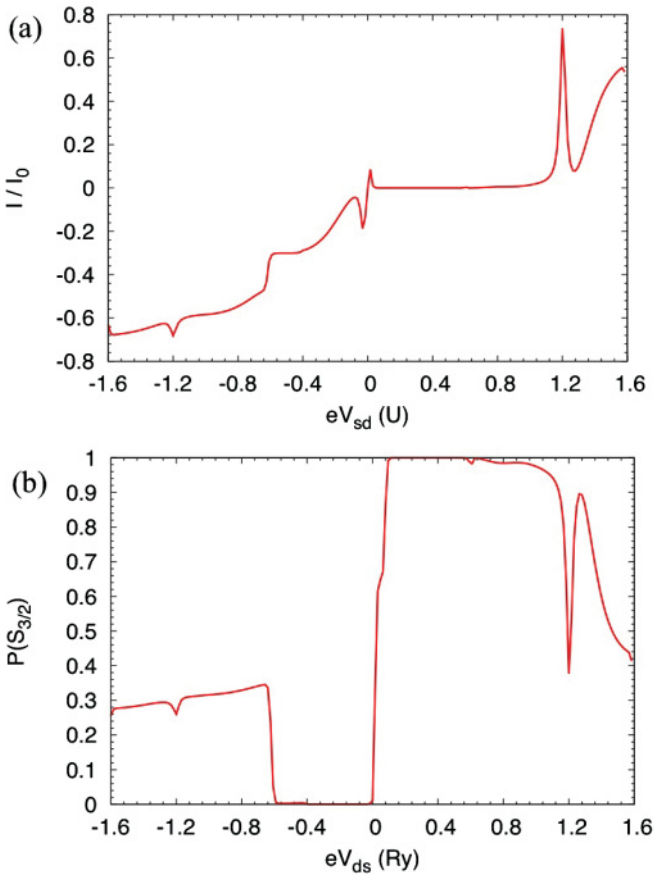

FIG. 9. (Color online) (a) The current of the LTQD at AQP as a function of V_{sd}. The current response is asymmetrical with respect to the bias direction. Similar to a DQD, current suppression is only observed in one direction of the bias. (b) The steady-state occupation probability for spin-3/2 states. The current suppression is associated with the spin-3/2 states.

For an electron to move from the left lead to the TQD, $E(\uparrow_1\uparrow_3) + \epsilon_e = E(\uparrow_1\uparrow_3\uparrow_4)$ for an electron energy $\varepsilon_e \leqslant \mu_L = eV_{sd}/2$. Thus, we get $eV_{sd} \geqslant 0.57U$. $E(\uparrow_1\uparrow_2\uparrow_3)$ is always lower than $E(\uparrow_1\uparrow_3\uparrow_4)$ for forward bias, so the relaxation from $|\uparrow_1\uparrow_3\uparrow_4\rangle$ to $|\uparrow_1\uparrow_2\uparrow_3\rangle$ is allowed. For the spin blockade to occur, the transition from $|\uparrow_1\uparrow_2\uparrow_3\rangle$ to $|\uparrow_1\uparrow_3\uparrow_4\rangle$ should not be possible by phonon emission. So, $E(\uparrow_1\uparrow_2\uparrow_3) < E(\uparrow_1\uparrow_3\uparrow_5)$, which leads to $eV_{sd} < 1.14U$. Therefore, the spin blockade regime is $0.57U \leqslant eV_{sd} < 1.14U$, which agrees very well with the numerical result in Fig. 7(a).

Next we consider the current of the LTQD at the AQP: (011), (012), (021), and (111). We again use a five-level Hubbard Hamiltonian for transport calculation. We assume that the quantum-dot potentials are now tuned such that the S orbital in the left dot, and the S and P orbitals in the central dot and the right dot become relevant for the electronic transport. In the weak tunnel coupling limit, the four charge configurations should be on resonance, and we set $E_1 = -V - V'$ and $E_2 = E_3 = -U - V$. Figure 9(a) shows the $I(V_{sd})$ of the TQD near the AQP. As expected, the current of the TQD near the AQP is very different under the two bias directions. Figure 9(b) confirms the spin blockade where the current is severely suppressed in the positive bias direction in Fig. 9(a). This phenomenon is in close analogy to the case of a DQD, and can be easily explained. In the positive bias, the electron is injected from the left dot. The transition from the $(0,1,1)$ triplet to a $(1,1,1)$ spin-3/2 state does not require the formation of onsite triplet. In the negative bias direction, the electron is injected from the right and transition from the $(0,1,1)$ triplet state to a spin-3/2 state requires the formation of an onsite triplet in the right dot. Therefore, before the bias threshold $\mu_R^* = E(0,1,2^*) - E(0,1,1)$, no spin blockade is expected to be formed. $(0,1,2^*)$ represents charge configuration in which one of the electrons occupies the P orbital in dot 3. When the applied bias exceeds the threshold, the condition $E(0,1,2^*) \geqslant E(0,2^*,1) \geqslant E(1,1,1)$ is also satisfied. Thus, either due to resonant tunneling or inelastic process, this additional electron can always be removed from the right lead. Therefore, there is no spin blockade in the negative bias direction. We remark that the spin blockade at AQP can be formed without the assistance of any relaxation mechanism. So, the spin blockade of a TQD at AQP is almost identical to the spin blockade in a DQD. Figure 10 presents the transport triangle in the parameter space $(E_1, E_2 = E_3)$ at a positive bias. In this figure, the light trail at the tip of the triangle is proportional to the onsite singlet-triplet gap in the central dot. This transport triangle, although generated under the specific condition $E_2 = E_3$, provides similar information that one can extract from the transport triangle for the DQD.

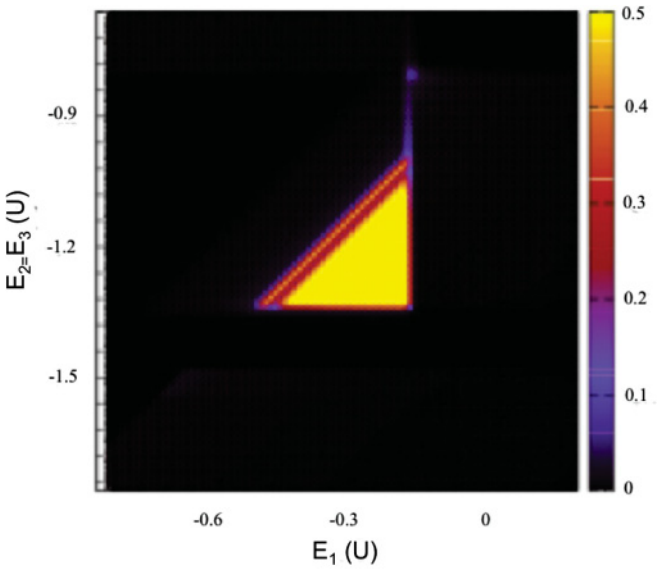

FIG. 10. (Color online) The current of the LTQD at AQP in the parameter space ($E_1, E_2 = E_3$).

IV. CONCLUSION

We presented a theory of electronic properties and transport through a LTQD around QPs. We showed that the spin blockade could serve as a spectroscopic tool for the detection of different spin states. Two different QPs containing the (1,1,1) configuration were discussed. A multiband Hubbard model with five levels was used to describe the electronic properties and investigate the spin-blockade phenomenon in the LTQD. For both QPs, strong current suppression and negative differential conductance were predicted. At the SQP, suppression in conductance was obtained under two different source-drain bias regimes. When the bias is small, the electronic transport involving spin-3/2 states takes place either via the S or P orbitals in the edge dot with comparable amplitude and results in a destructive interference. In the high-bias regime where electron tunnels onto the P orbital in the edge dot, spin blockade is facilitated by spin-conserving relaxation mechanisms, such as interaction with LA phonons studied here, and formation of the trap state. At the SQP, the spin-blockade phenomenon is bidirectional, in contrast with the spin blockade in a DQD. We also discussed spin blockade at the AQP. The spin-blockade formation and lifting in this case is in close analogy to the DQD case. The formation of the spin blockade does not involve any onsite triplets, only the lifting of the spin blockade requires the access to the onsite triplet states in the transport window. Similar to the DQD, the spin-blockade phenomenon at AQP only occurs in one bias direction.

ACKNOWLEDGEMENT

The authors thank L. Gaudreau, G. Granger, and A. Sachrajda for discussion and NSERC, QUANTUMWORKS, CIFAR, NRC-CNRS CRP, NRC-NSERC-BDC Nanotechnology project and OGS for financial support.

[1] M. Ciorga, A. S. Sachrajda, P. Hawrylak, C. Gould, P. Zawadzki, S. Jullian, Y. Feng, and Z. Wasilewski, Phys. Rev. B **61**, R16315 (2000).
[2] P. Hawrylak, Phys. Rev. B **60**, 5597 (1999).
[3] R. Hanson, J. R. Petta, S. Tarucha, and L. M. K. Vandersypen, Rev. Mod. Phys. **79**, 1217 (2007).
[4] F. Koppens, C. Buizert, K. Tielrooij, and I. Vink, Nature (London) **442**, 766 (2006).
[5] K. C. Nowack, F. H. L. Koppens, Y. V. Nazarov, and L. M. K. Vandersypen, Science **318**, 1430 (2007).
[6] M. Pioro-Ladrière, T. Obata, Y. Tokura, Y. S. Shin, T. Kubo, K. Yoshida, T. Taniyama, and S. Tarucha, Nat. Phys. **4**, 776 (2008).
[7] L. Gaudreau, A. Kam, G. Granger, S. A. Studenikin, P. Zawadzki, and A. S. Sachrajda, Appl. Phys. Lett. **95**, 193101 (2009).
[8] E. A. Laird, J. M. Taylor, D. P. DiVincenzo, C. M. Marcus, M. P. Hanson, and A. C. Gossard, Phys. Rev. B **82**, 075403 (2010).
[9] S. Amaha, T. Hatano, T. Kubo, S. Teraoka, Y. Tokura, S. Taruch, and D. G. Austing, Appl. Phys. Lett. **94**, 092103 (2009).
[10] M. Korkusinski and P. Hawrylak, in *Semiconductor Quantum Bits*, edited by O. Benson and F. Henneberger (World Scientific, Singapore, 2008).
[11] J. Petta, A. Johnson, J. Taylor, E. Laird, A. Yacoby, M. D. Lukin, C. M. Marcus, and M. P. Hanson, Science **309**, 2180 (2005).
[12] A. C. Johnson, J. R. Petta, C. M. Marcus, M. P. Hanson, and A. C. Gossard, Phys. Rev. B **72**, 165308 (2005).
[13] K. Ono, D. G. Austing, Y. Tokura, and S. Tarucha, Science **297**, 1313 (2002).
[14] J. Fransson, New J. Phys. **8**, 114 (2006).
[15] J. Fransson and M. Rasander, Phys. Rev. B **73**, 205333 (2006).
[16] G. Granger, L. Gaudreau, A. Kam, M. Pioro-Ladrière, S. A. Studeniken, Z. R. Wazilewzki, P. Zawadski, and A. S. Sachrajda, Phys. Rev. B **82**, 075304 (2010).
[17] M. Korkusinski, I. P. Gimenez, P. Hawrylak, L. Gaudreau, S. A. Studenikin, and A. S. Sachrajda, Phys. Rev. B **75**, 115301 (2007).
[18] K. Grove-Rasmussen, H. I. Jørgensen, T. Hayashi, P. E. Lindelof, and T. Fujisawa, Nano Lett. **8**, 1055 (2008).
[19] L. Gaudreau, G. Granger, A. Kam, G. C. Aers, S. A. Studenikin, P. Zawadzki, M. Pioro-Ladriére, Z. R. Wasilewski, and A. S. Sachrajda, Nature Phys. **8**, 54 (2012).
[20] Y. P. Shim, F. Delgado, and P. Hawrylak, Phys. Rev. B **80**, 115305 (2009).
[21] F. Delgado, Y. Shim, M. Korkusinski, L. Gaudreau, S. A. Studenikin, A. S. Sachrajda, and P. Hawrylak, Phys. Rev. Lett. **101**, 226810 (2008).
[22] D. DiVincenzo, D. Bacon, J. Kempe, and G. Burkard, Nature (London) **408**, 339 (2000).
[23] P. Hawrylak and M. Korkusinski, Solid State Commun. **136**, 508 (2005).
[24] C.-Y. Hsieh and P. Hawrylak, Phys. Rev. B **82**, 205311 (2010).
[25] Y.-P. Shim, A. Sharma, C.-Y. Hsieh, and P. Hawrylak, Solid State Commun. **150**, 2065 (2010).

[26] Y.-P. Shim and P. Hawrylak, Phys. Rev. B **78**, 165317 (2008).
[27] B. Röthlisberger, J. Lehmann, D. S. Saraga, P. Traber, and D. Loss, Phys. Rev. Lett. **100**, 100502 (2008).
[28] A. Sharma and P. Hawrylak, Phys. Rev. B **83**, 125311 (2011).
[29] M. Busl, R. Sánchez, and G. Platero, Phys. Rev. B **81**, 121306(R) (2010).
[30] I. Weymann, B. R. Bułka, and J. Barnaś, Phys. Rev. B **83**, 195302 (2011).
[31] K. Ingersent, A. W. W. Ludwig, and I. Affleck, Phys. Rev. Lett. **95**, 257204 (2005).
[32] R. Žitko and J. Bonča, Phys. Rev. Lett. **98**, 047203 (2007).
[33] A. M. Lobos and A. A. Aligia, Phys. Rev. B **74**, 165417 (2006).
[34] A. D. Greentree, J. H. Cole, A. R. Hamilton, and L. C. L. Hollenberg, Phys. Rev. B **70**, 235317 (2004).
[35] C. Emary, Phys. Rev. B **76**, 245319 (2007).
[36] I. Puerto Gimenez, M. Korkusinski, and P. Hawrylak, Phys. Rev. B **76**, 075336 (2007).
[37] I. P. Gimenez, C.-Y. Hsieh, M. Korkusinski, and P. Hawrylak, Phys. Rev. B **76**, 075336 (2007).
[38] B. Muralidharan and S. Datta, Phys. Rev. B **76**, 035432 (2007).
[39] M. Florescu and P. Hawrylak, Phys. Rev. B **73**, 045304 (2006).
[40] J. Iñarrea, G. Platero, and A. H. MacDonald, Phys. Rev. B **76**, 085329 (2007).
[41] B. Michaelis, C. Emary, and C. W. J. Beenakker, Europhys. Lett. **73**, 1 (2006).
[42] A. D. Greentree, A. R. Hamilton, and F. Green, Phys. Rev. B **70**, 041305(R) (2004).
[43] F. Qassemi, W. A. Coish, and F. K. Wilhelm, Phys. Rev. Lett. **102**, 176806 (2009).
[44] V. N. Golovach and D. Loss, Phys. Rev. B **69**, 245327 (2004).
[45] E. Vaz and J. Kyriakidis, J. Chem. Phys. **129**, 024903 (2008).
[46] T. Hansen, V. Mujica, and M. A. Ratner, Nano Lett. **8**, 3525 (2008).
[47] J. König, H. Schoeller, and G. Schön, Phys. Rev. Lett. **78**, 4482 (1997).
[48] A. Donarini, G. Begemann, and M. Grifoni, Phys. Rev. B **82**, 125451 (2010).